The Subgrid Velocity Scale in the Bulk Aerodynamic Relationship for Spatially Averaged Scalar Fluxes

L. MAHRT AND JIELUN SUN

College of Oceanic and Atmospheric Sciences, Oregon State University, Corvallis, Oregon

ABSTRACT

The exchange coefficients for area-averaged surface fluxes can become anomalously large when the large-scale flow is weak and significant fluxes of heat and moisture are driven by mesoscale motions within the averaging or subgrid area. To prevent this erratic behavior of the exchange coefficient, the "subgrid velocity scale" must be included to account for generation of turbulent fluxes by subgrid mesoscale motions. This velocity scale is obtained by spatially averaging the local time-averaged velocity used in the bulk aerodynamic relationship. The subgrid velocity scale is distinct from the free convection velocity scale included in the bulk aerodynamic relationship to represent transport induced by convectively driven boundary-layer-scale eddies (Godfrey and Beljaars; Beljaars). The formulation of Godfrey and Beljaars is derived by time averaging the velocity scale of the bulk aerodynamic relationship.

The behavior of the subgrid velocity scale is explored using data from five different field programs. Ubiquitous "nameless" mesoscale motions of unknown origin are found in all of the datasets. The addition of the subgrid velocity scale reduces the dependence of the exchange coefficients on grid size. Based on the data analysis, the subgrid velocity scale increases with grid size and contains a contribution due to surface heterogeneity.

1. Introduction

The local surface flux is often formulated in terms of the bulk aerodynamic relationship. This formulation is simple and practical and therefore widely used. Application of the bulk aerodynamic formulation and attendant similarity theories for the prediction of the exchange coefficient suffer from several problems that may require generalization of the formula. To introduce these problems, the bulk aerodynamic formulation is written as

$$\overline{w'\phi'} = C_\phi(z)\overline{V(z)}[\overline{\phi_{sfc}} - \overline{\phi(z)}], \qquad (1)$$

where $\overline{V(z)}$ is a time average of the wind speed, $\overline{\phi_{sfc}}$ is the time-averaged surface value of the transported variable, and $\overline{\phi(z)}$ is the time-averaged transported variable at the observational level or the first model level. With stationary homogeneous conditions, the exchange coefficient $C_\phi(z)$ is normally predicted from Monin–Obukhov similarity theory as a function of stability, surface roughness height, and observation height z.

The surface exchange coefficient based on Monin–Obukhov similarity theory relates the heat flux to the surface temperature at the roughness height. In practice

this similarity theory is normally applied using the surface radiation temperature or, analogously, the temperature computed from the surface energy budget. However, the roughness length for heat used in concert with Monin–Obukhov similarity theory and surface radiation temperature becomes extremely small over heated surfaces (Sugita and Brutsaert 1990). Sun and Mahrt (1995) show that this radiative roughness length is not systematically related to the actual roughness characteristics of the surface. This difficulty is due to the fact that Monin–Obukhov theory is not calibrated for use of the surface radiation temperature or the temperature computed from the surface energy balance.

The bulk aerodynamic formulation is used to predict fluxes spatially averaged over a grid area even though the similarity prediction of the exchange coefficient is based on local time-averaged data over homogeneous surfaces. In numerical models, the bulk aerodynamic relationship is expressed in terms of the speed of the wind vector based on the wind components spatially averaged over the grid area. This speed may be significantly smaller than the spatial average of the wind speed itself. In fact, the speed of the spatially averaged wind vector may nearly vanish, yet spatially averaged scalar fluxes remain significantly nonzero. This situation requires that the corresponding exchange coefficient approaches very large values. As an additional consequence, the exchange coefficients for the spatially averaged flow become scale dependent (Mahrt and Sun 1995).

Corresponding author address: Dr. Larry Mahrt, Oceanic and Atmospheric Sciences, Oregon State University, Corvallis, OR 97331-2209.

Models sometimes pragmatically address the problem of vanishing large-scale flow by either

1) specifying a minimum allowed wind speed,

2) modifying the stability dependence of C_ϕ such that the product of C_ϕ and the wind speed approaches a nonzero free-convection constant as the wind speed approaches zero [see Louis 1979, Eq. (14)], or

3) generalizing the mean velocity scale.

As an example of the third approach, Beljaars (1995) supplements the speed of the time-averaged wind vector with the free convection velocity scale in the surface flux formulation to account for generation of flux by convective circulations.

To examine the formulation of grid-averaged surface fluxes, the bulk aerodynamic relationship is spatially averaged in section 3. The resulting velocity scale in the bulk aerodynamic relationship is shown to include a contribution from unresolved subgrid mesoscale motions. The data used to evaluate the resulting bulk aerodynamic formulation and effective exchange coefficient for spatially averaged fluxes are described in section 4. The dependence of the effective exchange coefficient on grid size is investigated in section 5, and the generalized velocity scale for the bulk aerodynamic formula is parameterized in section 6. With this generalized velocity scale, the corresponding exchange coefficient for the spatially averaged flow $C_{\phi\text{eff}}$ is less sensitive to the spatial averaging scale (grid size) and more amenable to similarity theory.

2. Local time averaging and the free convection limit

The bulk aerodynamic formulation can be expressed in terms of the time average of the instantaneous wind speed

$$\bar{V} = \overline{(u^2 + v^2)^{1/2}} \qquad (2)$$

or the speed computed from the time-averaged wind components (vector average)

$$|\bar{\mathbf{V}}| = (\bar{u}^2 + \bar{v}^2)^{1/2}, \qquad (3)$$

where the overbar is a simple time average.

The bulk aerodynamic relationship based on the time average of the wind speed is expressed in (1), while the bulk aerodynamic relationship in terms of the vector-averaged wind is written as

$$\overline{w'\phi'} = \hat{C}_\phi |\bar{\mathbf{V}}| [\bar{\phi}_{\text{sfc}} - \overline{\phi(z)}], \qquad (4)$$

where $\hat{C}_\phi$ is an exchange coefficient defined by (4). Since the speed of the time-averaged wind vector is less than the time average of the instantaneous speed, $\hat{C}_\phi$ must be greater than the exchange coefficient based on the average of the instantaneous speed, C_ϕ [Eq. (1)]. However, the differences are small except in the case of weak winds and strong surface heating where the instantaneous speed is dominated by convectively

driven circulations. In this limit, $\hat{C}_\phi$ must become large so that the product $\hat{C}_\phi |\bar{\mathbf{V}}|$ remains finite as $|\bar{\mathbf{V}}|$ approaches zero.

a. Averaging the instantaneous speed

The previous use of the free convection velocity scale in the bulk aerodynamic velocity scale can be derived for the case where the time average of the wind speed is replaced by the speed of the time-averaged wind vector in order to accommodate numerical models. The following development shows which assumptions allow derivation of the generalized bulk aerodynamic relationship in Godfrey and Beljaars (1991) and Beljaars (1995).

The most straightforward derivation begins by time averaging the square of the instantaneous speed, expressed as

$$\overline{V^2} = \overline{(\bar{u}^2 + 2\bar{u}u' + u'^2 + \bar{v}^2 + 2\bar{v}v' + v'^2)}, \qquad (5)$$

where the prime quantities are turbulent fluctuations from the time average. For simple unweighted averaging, the cross terms $2\bar{u}u'$ and $2\bar{v}v'$ vanish. The remaining perturbation variance terms are a function of the surface friction velocity u_* and the free convection velocity w_*, in which case (5) can be parameterized as

$$\overline{V^2} = |\bar{\mathbf{V}}|^2 + g(|\bar{\mathbf{V}}|, u_*, w_*). \qquad (6)$$

Here $g(|\bar{\mathbf{V}}|, u_*, w_*)$ is analogous to the gustiness factor in Godfrey and Beljaars (1991), which is important in the limit of small-vector-averaged wind speed. Since the turbulence velocity variance in (5) is important only with weak winds (small $|\bar{\mathbf{V}}|$) and significant surface heating, the function g can be formulated in terms of a quadratic function of w_*. Neglecting the difference between the average of the square root and the square root of the average, (6) becomes

$$\overline{V^2} = [|\bar{\mathbf{V}}|^2 + (\beta w_*)^2]. \qquad (7)$$

Using this velocity scale, the bulk aerodynamic relationship (1) can be expressed in terms of the speed of the time-averaged wind vector in the form

$$\overline{w'\phi'} = C_\phi [|\bar{\mathbf{V}}|^2 + (\beta w_*)^2]^{1/2} [\bar{\phi}_{\text{sfc}} - \overline{\phi(z)}]. \qquad (8)$$

The above development of (8) provides some justification for introducing w_* as an additional velocity scale but does not offer rigorous justification for the exact form of the generalized velocity scale. The addition of the free convection velocity scale was conceptually motivated by Businger (1973), who defined a minimum Obukhov length where u_* was replaced by a function of the free convection velocity scale (Liu et al. 1979; Schumann 1988). Godfrey and Beljaars (1991) and Beljaars (1995) proposed use of an additional velocity scale in terms of surface flux generated by the horizontal velocity fluctuations induced by boundary-layer-scale eddies.

In fact, the addition of the free convection velocity scale is similar to modifying the stability function of the exchange coefficient, as can be shown by factoring out the speed of time-averaged wind vector $|\overline{\mathbf{V}}|$ in (8), in which case

$$\overline{w'\phi'} = C_\phi(1 + \hat{\mathrm{Ri}})^{1/2}|\overline{\mathbf{V}}|[\overline{\phi_{\mathrm{sfc}}} - \overline{\phi(z)}], \quad (9)$$

where

$$\hat{\mathrm{Ri}} = \frac{(\beta w_*)^2}{|\overline{\mathbf{V}}|^2}. \quad (10)$$

The Richardson number in the form $\hat{\mathrm{Ri}}$ is valid only for the unstable case since both w_* and $\hat{\mathrm{Ri}}$ are undefined in the stable case. Equation (9) can be transformed to the bulk aerodynamic formula (4) by defining the exchange coefficient $\hat{C}_\phi = C_\phi(1 + \hat{\mathrm{Ri}})^{1/2}$. Expressing (9) in terms of the exchange coefficient $\hat{C}_\phi$ is analogous to approach 2 in the introduction since the product $\hat{C}_\phi|\overline{\mathbf{V}}|$ approaches a nonzero constant in the limit of vanishing $|\overline{\mathbf{V}}|$. In fact, the functional dependence on the Richardson number in (9) is similar to that in Louis (1979) for the free convection limit. This comparison shows that the approaches of Louis (1979) and Godfrey and Beljaars (1991) are asymptotically similar in terms of the dependence on stability. However, the two approaches are numerically different, and the Louis scheme underestimates fluxes in the free convection limit (Miller et al. 1992) without further adjustment. Equation (9) also indicates that using approach 2 and the addition of the free convection velocity scale are redundant.

b. Explicit form of buoyancy velocity

The formulation for the generalized velocity scale in (8) can be converted to an explicit form where the right-hand side does not depend on the heat flux by replacing w_* with the "buoyancy velocity scale" (Stull 1994)

$$w_B = \left(\frac{g}{\theta_v} z_i \Delta\theta_B\right)^{1/2}, \quad (11)$$

where z_i is the depth of the boundary layer and $\Delta\theta_B$ is the difference between the virtual potential temperature corresponding to the surface radiation temperature and the virtual potential temperature of the mixed layer. This temperature difference must be positive for application of (11). Using the velocity scale w_B, the bulk aerodynamic formula for the heat flux from Stull (1994) is

$$\overline{w'\theta'} = (C_{HML}M_{ML} + b_H w_B)[\overline{\theta_{\mathrm{sfc}}} - \overline{\theta(z)}], \quad (12)$$

where $C_{HML} = 0.001$, $b_H = 0.00025$, M_{ML} is the speed of the mean wind in the mixed layer, and $\overline{\theta_{\mathrm{sfc}}}$ is the surface radiation temperature. The free convection form of (12), where M_{ML} approaches zero [see Stull 1994, his (Eq. 17)], is analogous to that of Sykes et al.

[1993 (Eq. 11)] if $C_{HML} = (\alpha_4)^{3/2}(z_s/z_i)^{3/2}$, where z_s is the depth of the surface layer, which in turn depends on surface roughness, and α_4 is a dimensionless coefficient defined in Sykes et al. (1993).

In (12), the buoyancy term $b_H w_B$ is linearly added to the wind speed term $C_{HML}M_{ML}$, whereas the buoyancy term is quadratically added to the wind speed in Godfrey and Beljaars (1991). Based on the datasets of this study, the ability of the two approaches to reduce the scale dependence of the exchange coefficients is similar (not shown here). Derivation of the quadratic form (7) requires fewer assumptions than the linear combination and will be used in this study.

For future use, a generalized free convection velocity scale is defined in flux form as

$$\langle w_{\mathrm{fc}}\rangle \equiv \beta\langle w_*\rangle, \quad (13)$$

and in explicit form as

$$\langle w_{\mathrm{fc}}\rangle \equiv b_H\langle w_B\rangle. \quad (14)$$

3. Subgrid velocity scale

Since similarity formulation of the bulk aerodynamic method relates the flux to the locally time-averaged speed, formulation of area-averaged turbulent fluxes requires an expression for the grid-area average of the locally time-averaged speed. Therefore, anticipating application to parameterization of grid-averaged surface fluxes, the time average of each wind component and the generalized free convection velocity scale [(13) and (14)] are decomposed into an average over the grid area ($\langle\overline{u}\rangle$, $\langle\overline{v}\rangle$, $\langle w_{\mathrm{fc}}\rangle$) and the deviation of the local time average from the area average (u^*, v^*, w_{fc}^*). Then,

$$\overline{u} = \langle\overline{u}\rangle + u^*$$

$$\overline{v} = \langle\overline{v}\rangle + v^* \quad (15)$$

$$w_{\mathrm{fc}} = \langle w_{\mathrm{fc}}\rangle + w_{\mathrm{fc}}^*. \quad (16)$$

The angle brackets define spatial averaging over a grid area of width Δx and represent the resolved flow in numerical models. [More precisely, only motions on a scale of $4\Delta x$ or greater are fully resolved (see Avissar 1990).]

Using decomposition (15), the square of the locally time-averaged wind speed (7) becomes

$$\overline{V}^2 = |\overline{\mathbf{V}}|^2 + w_{\mathrm{fc}}^2 = (\langle\overline{u}\rangle + u^*)^2$$

$$+ (\langle\overline{v}\rangle + v^*)^2 + (\langle w_{\mathrm{fc}}\rangle + w_{\mathrm{fc}}^*)^2. \quad (17)$$

Spatially averaging the square of the speed (17) over the grid area

$$\langle\overline{V}^2\rangle = |\langle\overline{\mathbf{V}}\rangle|^2 + \langle w_{\mathrm{fc}}\rangle^2 + \langle u^{*2} + v^{*2} + w_{\mathrm{fc}}^{*2}\rangle, \quad (18)$$

where the speed of the spatially averaged wind vector is defined as

$$|\langle \bar{\mathbf{V}} \rangle| = (\langle \bar{u} \rangle^2 + \langle \bar{v} \rangle^2)^{1/2}. \quad (19)$$

Numerical models determine only the speed of the spatially averaged wind vector $|\langle \bar{\mathbf{V}} \rangle|$ (first term on the right-hand side of 18) based on the grid-averaged (resolved) wind components computed from the equations of motion. However, the local flux is related to the local time-averaged wind so that the spatially averaged flux should be related to the spatial average of the local time-averaged wind, which would require evaluation of the entire right-hand side of (18).

To show the difference between these two different spatially averaged winds, an example of diverging mesoscale flow is sketched in Fig. 1, qualitatively based on data described in section 4. Here the spatially averaged wind vector nearly vanishes when the grid area includes both branches of the mesoscale flow. That is, the two branches of the outflow cancel when averaging the wind components over the grid area, leading to very small spatially averaged wind components, so that $|\langle \bar{\mathbf{V}} \rangle| \ll \langle \bar{V} \rangle$. However, when the grid size is small compared to the mesoscale circulation, the mesoscale flow is resolved and $|\langle \bar{\mathbf{V}} \rangle| \approx \langle \bar{V} \rangle$. Since the spatially averaged moisture and heat fluxes are about the same for both grid sizes, the exchange coefficient for the usual bulk aerodynamic relationship must be much larger in the case of larger grid size. Consequently, the exchange coefficient not only becomes large in the case of vanishing large-scale flow but depends on grid size. Therefore, use of the speed of the spatially averaged wind vector ($|\langle \bar{\mathbf{V}} \rangle|$) in numerical models requires scale-dependent exchange coefficients in the case of weak large-scale flow.

Alternatively, this study will parameterize the difference between the speed of the resolved flow and the spatial average of the local time-averaged speed by simplifying (18). Neglecting the spatial variations of the free convection velocity scale and neglecting the difference between the spatial average of the square root and the square root of the spatial average (found to be a good approximation for the present data), (18) simplifies to

$$\langle \bar{V} \rangle^2 = |\langle \bar{\mathbf{V}} \rangle|^2 + \langle w_{\mathrm{fc}} \rangle^2 + V_{\mathrm{sg}}^2, \quad (20)$$

where the *subgrid velocity scale* is defined as

$$V_{\mathrm{sg}}^2 \equiv \langle u^{*2} \rangle + \langle v^{*2} \rangle. \quad (21)$$

The subgrid velocity scale represents the generation of turbulent flux by the unresolved subgrid mesoscale flow.

Using the velocity scale (20), the bulk aerodynamic formulation for the spatially averaged flux becomes

$$\langle \overline{w'\phi'} \rangle = C_{\phi\mathrm{eff}}(|\langle \bar{\mathbf{V}} \rangle|^2 + \langle w_{\mathrm{fc}} \rangle^2 + V_{\mathrm{sg}}^2)^{1/2}$$
$$\times [\langle \overline{\phi_{\mathrm{sfc}}} \rangle - \langle \overline{\phi(z)} \rangle]. \quad (22)$$
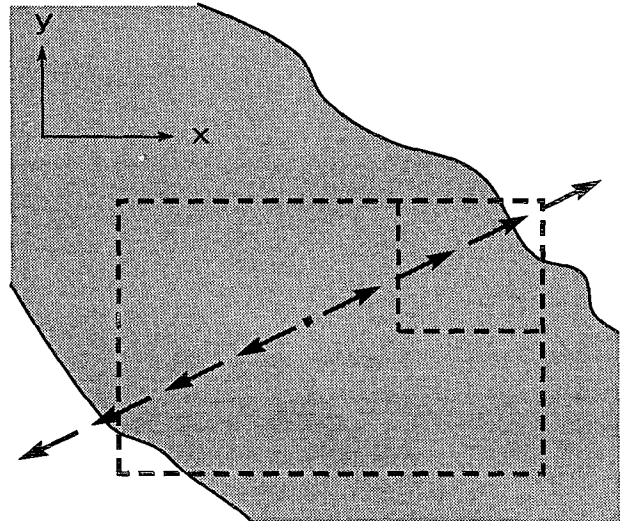

FIG. 1. A schematic of the diverging mesoscale flow over the irrigated area (shaded area) qualitatively based on CODE flight 19 (section 4). For the larger grid box (large dashed box), the spatially averaged wind components nearly vanish. For the smaller grid box, the mesoscale flow is resolved and the spatially averaged wind components are significantly nonzero.

Here $C_{\phi\mathrm{eff}}$ is an *effective exchange coefficient* defined by (22), which relates spatially averaged fluxes to the spatially averaged air–surface differences.

The effective exchange coefficient could be estimated by partitioning C_ϕ, ϕ_{sfc}, and $\phi(z)$ into area-averaged parts and deviations from the area average as in (15), substituting into the bulk aerodynamic relationship and then spatially averaging the entire relationship. This approach leads to "extra" Reynolds terms associated with spatial correlations between $|\bar{\mathbf{V}}|$, C_ϕ, ϕ_{sfc}, and $\phi(z)$ (Esbensen and Reynolds 1981). This study will follow a simpler approach and evaluate $C_{\phi\mathrm{eff}}$ directly from data. The data analysis in section 5 will show that the addition of the subgrid velocity scale significantly reduces the dependence of the effective exchange coefficient on grid size or averaging scale so that similarity theory might be used to estimate $C_{\phi\mathrm{eff}}$.

The dependence of the drag coefficient on averaging scale is more complicated than the exchange coefficient for scalar quantities because the surface stress is a vector quantity and is sometimes reduced by spatial averaging, as occurred for the wind vector in Fig. 1. Because of this averaging effect and the fact that the surface drag is more aligned with the mean shear vector than the mean wind vector, the drag coefficient for the spatially averaged momentum flux depends on averaging scale in a way that is not systematic between studies. The mesoscale flux is also influenced by the mesoscale pressure field. In a case study of strong surface heterogeneity, Mahrt et al. (1994a) found that the momentum flux is significantly modulated by transient mesoscale motions, while the heat and moisture fluxes

TABLE 1. Data.

Field program	Length of flight (km)	Number of runs	Observation level (m)	References
CODE flight 13	30	8	30	MacPherson (1992)
CODE flight 19	30	8	30	MacPherson (1992)
HAPEX, 19, 25 May	120	6	125	Mahrt (1991)
buFex, Lake King	50	6	12	Lyons et al. (1993)
TOGA COARE	70	24	40	TCIPO (1993)
Pre-BOREAS	40	6	50	NASA (1994)

are characterized by a simpler quasi-stationary spatial distribution dictated by surface heterogeneity. This study will concentrate on the spatially averaged heat and moisture fluxes.

Since V_{sg} represents the influence of all motions between the largest turbulent scales and the scale of the spatial averaging, its value is proportional to the scale of spatial averaging or grid size Δx, as is shown in section 5. To organize the data analysis in section 6, the subgrid velocity scale can be tentatively formulated as

$$V_{sg}^2(\Delta T_{sfc}, \mathbf{V}, \Delta x)$$

$$= V_{sgl}^2(\Delta T_{sfc}, \mathbf{V}, \Delta x) + V_{sgT}^2(\Delta x) + V_{sgS}^2. \quad (23)$$

The first term on the right-hand side represents the influence of surface heterogeneity, where ΔT_{sfc} is some measure of the variability of surface temperature, to be defined later. The second term represents the general influence of transient mesoscale motions found to increase with grid size (section 6). The last term represents the influence of well-defined mesoscale events such as organized moist convection and sea breezes and is not explicitly considered in this study. Formulation of V_{sg} will be constructed in section 6 by analyzing data from five different field programs discussed in the next section.

4. Data

To evaluate the velocity scale in the bulk aerodynamic formulation, data from five different field programs are analyzed (Table 1). The data from the California Ozone Deposition Experiment (CODE) is described in Sun and Mahrt (1994) and references therein. In this field program, strong spatial variations of surface vegetation and soil moisture due to irrigation significantly influence the observed flow and generate inland breezes with weak large-scale flow. The data contain eight repeated flights over the same flight track, about 30 km long at 30 m above ground, on each of the two flight days. This dataset provides the largest available sample size of near-surface fluxes over heterogeneous terrain.

Data from the pre-Boreal Ecosystem–Atmosphere Study (pre-BOREAS) consist of Canadian NRC Twin Otter flights over a relatively flat forest. The data were taken under cloudy conditions along the "Candle Lake track" (NASA 1994). Data from the bunny fence experiment (buFex) were collected over a region partly occupied by mixed agricultural land use and partly by a semiarid surface with native vegetation (Lyons et al. 1993). The surface heterogeneity in buFex did not generate observable mesoscale motion, because of significant large-scale flow.

The data from the Hydrological and Atmospheric Pilot Experiment (HAPEX) consist of six repeated flights of the National Center for Atmospheric Research (NCAR) King Air over a 125-km flight tract above a flat pine forest in southwest France (Les Landes), providing one of the largest sample sizes of turbulence and small mesoscale motions over land. These data were collected on each of two individual flight days. The Tropical Oceans Global Atmosphere Coupled Ocean–Atmosphere Response Experiment (TOGA COARE) data consist of 24 NCAR Electra flights over the western equatorial Pacific with a track length of typically 60–70 km. These data include a range of conditions from relatively undisturbed conditions to well-organized intense moist convection.

For each flight over land, the runs are aligned and the influence of variable aircraft speed is reduced by stretching (or contracting) and translating each record based on ground markers. For CODE, the ground markers are determined from the aircraft measured NDVI (normalized difference vegetation index) (Tucker 1979). For the other flights, the ground markers are determined from radiometrically measured terrain heights and the surface radiation temperature. Since the TOGA COARE flights are over the sea, the flights are not aligned.

The aircraft runs are divided into 5-km segments. Fluctuations are computed from the 5-km unweighted averages. This averaging operator separates the "turbulence" from the mesoscale part and in some sense is a substitute for a local time average. The choice of 5 km as a partitioning scale is somewhat arbitrary and theoretically should be proportional to height above ground, instability, and the boundary layer depth. The choice of 5 km attempts to eliminate the mesoscale flux that can be of either sign with respect to the turbulence flux and is therefore not represented by the bulk aero-
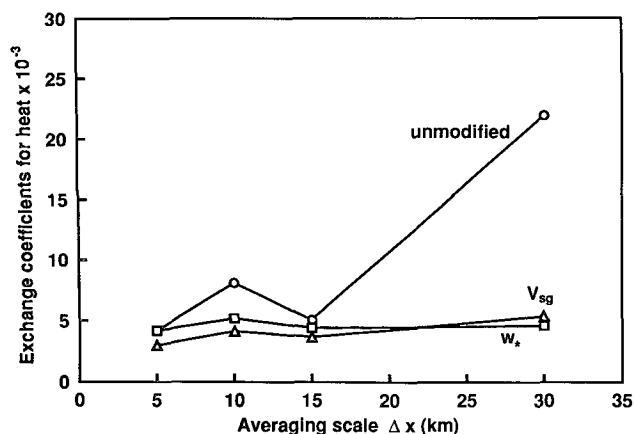
FIG. 2. The effective exchange coefficient for heat from CODE flight 19 as a function of averaging scale. The models are the unmodified bulk aerodynamic formulation (circles), inclusion of w_* in the velocity scale (squares), and inclusion of V_{sg} in the velocity scale (diamonds).

dynamic relationship. With a smaller partitioning scale, the so-called "mean" flow contains variations on scales that are too small to maintain equilibrium turbulence, and the computed turbulent flux would be more contaminated by small sample size. To compute the spatially averaged flux, the products of the perturbations are averaged over different values of the averaging scale Δx. Regardless of the averaging scale Δx, the perturbation quantities are always computed as deviations from the 5-km mean.

The speed of the spatial average of the instantaneous wind vector $|\langle V \rangle|$, measured by the aircraft, will be used as an estimate of the speed of the spatial average of the local time average $|\langle \bar{V} \rangle|$, needed in the bulk aerodynamic relationship. The heat flux, surface radiation temperature, $|\langle V \rangle|$, and V_{sg} are computed for each record subsegment of width Δx. The exchange coefficient for heat is then computed from these values for each subsegment. For a given value of Δx, subsegment values of the exchange coefficient are averaged over all of the flight legs for a given flight day to form just one value for each value of Δx, symbolized as $[C_{\phi eff}]$. The square brackets denote averaging subsegment values over a given flight day. For TOGA COARE, the values of the exchange coefficient, for a given value of Δx, are averaged over all of the flight days. The effective exchange coefficients for moisture are computed in the same way as those for heat, where the surface specific humidity is assigned to be the saturation value at the surface radiation temperature.

5. Scale dependence of the exchange coefficients

Sections 2 and 3 suggested the use of additional velocity scales in the bulk aerodynamic relationship. Failure to generalize the velocity scale of the bulk aero-

dynamic relationship in the case of weak large-scale flow could require exchange coefficients that are much larger than those predicted by similarity theory. Such large values of the exchange coefficients will be found from data for CODE flight 19 where the large-scale flow is weak and the surface heterogeneity generates well-defined mesoscale flow. For this case, the speed of the spatially averaged wind vector ($|\langle V \rangle|$) becomes small when averaging over the scale of the irrigated area, as is schematically pictured in Fig. 1. The two branches of the outflow from the irrigated area (irrigation breeze) partially cancel when spatially averaging the velocity components.

The averaged exchange coefficients $[C_{\phi eff}(\Delta x)]$ are computed as described in section 4 for the following different forms of the generalized velocity scale in (22) using the flux form of the free convection velocity scale:

1) the unmodified bulk aerodynamic formulation for numerical models ($\beta = 0$, $V_{sg} = 0$),

2) the free convection modification ($\beta = 1$, $V_{sg} = 0$), and

3) the modification to include subgrid mesoscale motions ($\beta = 0$, $V_{sg} \neq 0$).

In cases where the virtual heat flux is negative, w_* is set to zero in the second model.

The exchange coefficient for CODE flight 19 for the unmodified formulation (model 1) becomes large (Figs. 2 and 3) as the grid averaging area exceeds the width of the irrigated area. These large values are necessary to compensate for the decreasing magnitude of the spatially averaged (resolved) flow $|\langle V \rangle|$ since the spatially averaged turbulent fluxes do not necessarily decrease with increasing averaging scale. The exchange coefficients for heat and moisture computed
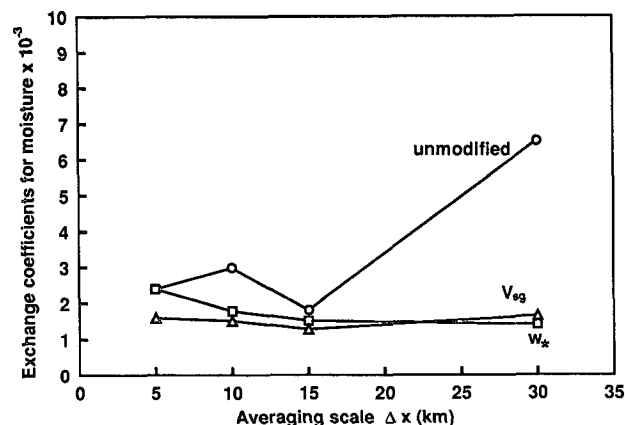

FIG. 3. The effective exchange coefficient for moisture from CODE flight 19 as a function of averaging scale. The models are the unmodified bulk aerodynamic formulation (circles), inclusion of w_* in the velocity scale (squares), and inclusion of V_{sg} in the velocity scale (diamonds).

from the other datasets generally show much less dependence on averaging scale.

Using either one of the generalized velocity scales (model 2 or 3) reduces the scale dependence of the exchange coefficient for CODE flight 19. *Any* additional, significantly nonzero velocity scale prevents the total velocity scale from becoming small as $|\langle V \rangle|$ becomes small. However, choosing the inner 15 km of the record occurring mainly over irrigated cotton in CODE flight 19, both $|\langle V \rangle|$ and w_* become small even though the turbulent moisture fluxes do not become small. The significant turbulent moisture flux is maintained by the diverging mesoscale flow. As a result, the exchange coefficient for the area-averaged moisture flux is significantly larger than that predicted by similarity theory, unless the bulk aerodynamic formulation includes the subgrid velocity scale V_{sg}.

When the above analyses of CODE data are repeated with natural sublegs based on land-use boundaries, greater scale dependence is captured at smaller averaging scales. As a result, the exchange coefficients for the unmodified formulation (model 1) begin to increase at smaller averaging scale Δx when compared to Figs. 2 and 3, where the exchange coefficients for the unmodified formulation increase mainly between the 15- and 30-km averaging scales. Dividing the surface area according to natural surface boundaries more effectively captures the impact of the heterogeneity. In numerical models, the boundaries of grid boxes are not chosen with respect to natural boundaries. Therefore, this study emphasizes the calculations based on arbitrarily chosen 5-km subrecords, beginning at the start of the flight track.

The exchange coefficient for heat predicted by the model of Stull (1994), defined by (12), was evaluated by using the temperature and wind speed at flight level as estimates of the mixed-layer-averaged values. The exchange coefficient for heat increases by about 30% when the averaging scale increases from 15 to 30 km. This increase is much less than the 300% increase for the unmodified bulk aerodynamic formulation (model 1). Therefore, the addition of the buoyancy velocity scale in (12) mathematically reduces the scale dependence of the exchange coefficient for the unstable case, because the total velocity scale does not become very small when the large-scale flow becomes weak.

6. Parameterization of the subgrid velocity scale

The subgrid velocity scale V_{sg} is estimated from (20) using 5-km averages for all of the datasets in Table 1. The subgrid velocity scale V_{sg} can be viewed as a bandpass filter of the horizontal velocity variance between the scales of 5 km and Δx. Depending on grid size, V_{sg} is typically about 0.5 m s^{-1} for those datasets with no strong effect of surface heterogeneity (open symbols, Fig. 4) and significantly larger for the two CODE flights (solid symbols, Fig. 4), where surface hetero-
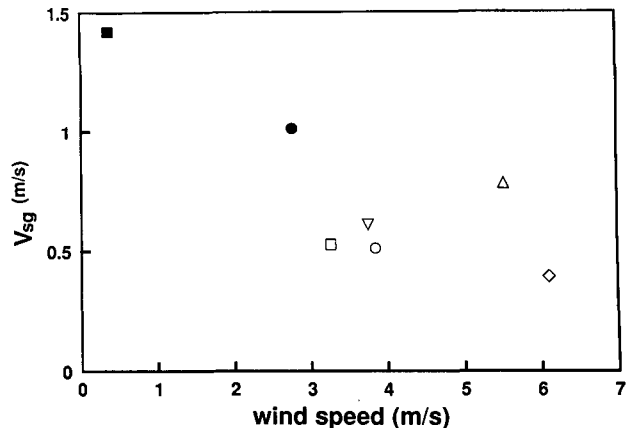

FIG. 4. The subgrid velocity scale as a function of the speed of the spatially averaged wind vector for $\Delta x = 30$ km for HAPEX flight 19 (open circle), HAPEX 25 (open square), buFex (triangle), pre-BOREAS (diamond), TOGA COARE (inverted triangle), CODE flight 13 (solid circle), and CODE flight 19 (solid square).

geneity is important. Each symbol in Fig. 4 represents V_{sg} averaged over all of the flight legs for the indicated field program or flight day.

a. Surface heterogeneity

Surface heterogeneity generates mesoscale spatial variation of air temperature corresponding to horizontal gradients of the hydrostatic perturbation pressure. This pressure gradient produces local mesoscale flow that in turn generates turbulence and turbulent transport. The magnitude of the mesoscale pressure perturbation at the surface is proportional to the depth and amplitude of the temperature perturbation, which usually increases with the horizontal scale of the heterogeneity. Smaller-scale temperature gradients fail to generate local flows, particularly with significant ambient airflow (Hechtel et al. 1990; Segal and Arritt 1992; Hadfield et al. 1992; Mahrt et al. 1994b).

The largest scale of the thermally generated mesoscale motions, not resolved by the numerical model, is proportional to the grid size Δx. Choosing the grid size as the length scale, the simplest subgrid velocity scale that represents the generation of mesoscale motions by surface heterogeneity can be constructed as

$$V_{sg}(\Delta T_{sfc}, |\langle V \rangle|, \Delta x) = C\left(\frac{g}{T_0} \Delta T_{sfc}\Delta x\right)^{1/2}, \quad (24)$$

where ΔT_{sfc} is a measure of the variation of surface radiation temperature, T_0 is the spatial average of the surface radiation temperature, and C is a decreasing nondimensional function of the large-scale wind speed $|\langle V \rangle|$. With this formulation, local motions generated by the surface heterogeneity are proportional to the surface temperature variation and the grid size.

The total value of the subgrid velocity scale (23) computed from the data is formulated as the sum of the transient part (section 6b) and the part due to surface heterogeneity (24). In section 6b, the transient part is nominally modeled as a function of the grid size and is approximately 0.55 m s^{-1} for Δx = 30 km (length of the flight track for CODE flight 19). Subtracting this modeled value of the transient part from the observed value of V_{sg} = 1.42 m s^{-1} for Δx = 30 km for CODE flight 19, the value of V_{sgI} is 0.87 m s^{-1}. Assigning ΔT_{sfc} to be the standard deviation of the 5-km averages of the surface radiation temperature for Δx = 30 km (approximately 7°C), the nondimensional function C in (24) is estimated to be 0.0104 with Δx = 30 km for CODE flight 19.

For CODE flight 13, the part of V_{sg} due to the surface heterogeneity is computed to be 0.47 m s^{-1}. The mesoscale motion organized by the surface heterogeneity for flight 13 takes the form of diffluence of the large-scale flow and is visibly weaker when compared to flight 19. Thus, an increase of large-scale flow from about 0.4 m s^{-1} for flight 19 to about 2.8 m s^{-1} for flight 13 significantly reduces the mesoscale flow driven by surface temperature variations. For CODE flight 13, the standard deviation of the 5-km-averaged surface radiative temperature is also about 7°C, and C is estimated to be about 0.0056 at Δx = 30 km.

The dependence of this function on the speed of the large-scale flow can be formulated as

$$C = C(0) \exp\left(-\frac{|\langle\mathbf{V}\rangle|}{V_{crit}}\right). \qquad (25)$$

An exact fit to the two CODE flights yields $C(0)$ = 0.015 and V_{crit} = 3.9 m s^{-1}. For the other field programs, ΔT_{sfc} is less than 2°C, the wind speed $|\langle\mathbf{V}\rangle|$ is stronger than that in CODE, and V_{sgI} is found to be unimportant within the accuracy of the measurements. Consequently, V_{sgI} will be assumed to be zero in the other field programs. The effect of surface heterogeneity might be stronger in mesoscale models where the corresponding mesoscale circulation does not have to compete with transient mesoscale motions. Furthermore, in mesoscale models, the surface heterogeneity is organized with respect to the horizontal boundaries of the model that typically employ periodic boundary conditions.

Application of (24) as a subgrid parameterization in large-scale numerical models would require representation of the subgrid variability of the surface radiation temperature ΔT_{sfc}, which is normally not available in existing numerical models. Information on ΔT_{sfc} might be deduced from real-time satellite data or from models that include some representation of subgrid variability of the surface conditions as in Wetzel and Chang (1988), Avissar and Pielke (1989), Claussen (1991), Ducoudré et al. (1993), and Huang and Lyons (1995).

b. Transient mesoscale motions

Significant mesoscale energy is present in all of the datasets in this study, whether or not surface heterogeneity is present. This subsection attempts to formulate the magnitude of the subgrid velocity scale due to transient mesoscale motions, V_{sgT}. The data from CODE are excluded from this formulation since the surface heterogeneity was dominant. Presumably V_{sgT} increases with record length (or grid size) since larger record length includes a larger range of mesoscale motions. In fact, V_{sgT} increases systematically with increasing grid size for all of the datasets (Fig. 5). The velocity scale V_{sgT} for the TOGA COARE data is a little stronger at large grid sizes compared to the overland cases. This may be due to mesoscale organization of both weak and intensive convective cloud systems in TOGA COARE. The velocity scale V_{sgT} is relatively small in the pre-BOREAS data, which were taken with nonconvective cloudy conditions. One can speculate that surface heating induces transient mesoscale circulations such as inertial gravity waves at the top of the boundary layer and augments V_{sgT} for the other overland cases. Differences in stability and flight level above ground, the failure of the turbulence to achieve equilibrium with the mean flow, and errors in the formulated dependence on Δx might also contribute to variations of V_{sgT}. The following analysis examines only the dependence of V_{sgT} on grid size.

The least squares fit of the log(V_{sgT}) to log(Δx) for the data in Fig. 5 yields the following relationship:

$$V_{sgT} = 0.32\left(\frac{\Delta x}{5} - 1\right)^{0.33}, \qquad (26)$$

where Δx is expressed in kilometers and V_{sgT} in meters per second. This relationship explains 71% of the variance of log(V_{sg}). With this formulation, the predicted
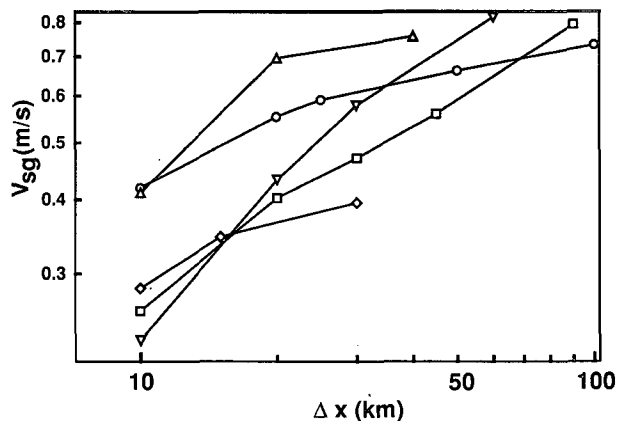

FIG. 5. The subgrid velocity scale V_{sg} as a function of the averaging length (simulated grid size) Δx for HAPEX flight 19 (circles), HAPEX flight 25 (squares), buFex (triangles), pre-BOREAS (diamonds), and TOGA COARE (inverted triangles).

V_{sgT} increases from 0.32 m s^{-1} at $\Delta x = 10$ km, to 0.85 m s^{-1} at $\Delta x = 100$ km, to 1.37 m s^{-1} at $\Delta x = 400$ km.

Depending on grid size, the subgrid velocity scale is significant only when the large-scale, vector-averaged flow is less than a few meters per second. Therefore, the subgrid velocity scale is important only for a small fraction of the time. However, in such cases the unmodified formulation, based on the spatially averaged wind vector, can lead to significant errors and erratic model behavior. Thus, some models contain safety "if" statements that prohibit very weak large-scale flow. The simplest possible model would be to specify a globally constant value of V_{sg} such as $V_{sg} = 0.5$ m s^{-1}. This value could be augmented to include the climatological effect of more organized mesoscale motion, excluded in most of the data analyzed here. Specification of constant V_{sg} could replace specification of a minimum wind speed (approach 1, introduction). A more flexible, but still simple approach is to use (26), which includes the dependence of V_{sg} on grid size.

Substituting (26) and (24) with decomposition (23) into the bulk aerodynamic relationship (22) yields

$$\langle w'\phi' \rangle = C_{\phi\text{eff}}\left\{ |\langle \mathbf{V}\rangle|^2 + \langle w_{fc}\rangle^2 \right.$$

$$\left. + \left[C^*\left(\frac{\Delta x}{5} - 1\right)^{0.33}\right]^2 + C^2\left(\frac{g}{T_0}\Delta T_{\text{sfc}}\Delta x\right)\right\}^{1/2}$$

$$\times [\langle \phi_{\text{sfc}}\rangle - \langle \phi(z)\rangle]. \quad (27)$$

The nondimensional function for the surface heterogeneity term C is a decreasing function of wind speed (25) and $C^* = 0.32$ m s^{-1} [see Eq. (26)]. This surface heterogeneity term must be neglected unless information is available on subgrid surface temperature variations. Although the above calculations have employed a large number of flight legs, (27) must be considered tentative. More data for cases of weak large-scale flow and cases of strong organized mesoscale motion are needed.

7. Conclusions and discussion

The value of the effective exchange coefficients for area-averaged fluxes can depend significantly on the scale of averaging for weak large-scale flow. This scale dependence of the exchange coefficient is partly related to turbulent fluxes generated by subgrid mesoscale circulations within the grid averaging area. In other terms, the speed of the wind vector, spatially averaged over the grid area, is sometimes significantly smaller than the spatial average of the speed, depending on the importance of mesoscale motions that are smaller than the grid size. As a result, exchange coefficients in the unmodified bulk aerodynamic relationship for weak large-scale flow become significantly scale dependent. For the CODE data (section 5), the exchange coeffi-

cients for heat and moisture increase dramatically with increasing averaging scale.

This scale dependence of the exchange coefficient is removed by including the *subgrid velocity scale* in the bulk aerodynamic formulation that accounts for turbulent flux generated by subgrid mesoscale motions. The subgrid velocity scale is derived in section 3 by spatially averaging the velocity scale in the bulk aerodynamic relationship. The inclusion of the subgrid velocity scale into the bulk aerodynamic formula is mathematically equivalent to replacing the resolved velocity (based on grid averaged velocity components) with the spatial average of the local time-averaged wind speed (section 3). Since the latter averaged speed is not available in numerical models, a parameterized subgrid velocity scale should be incorporated in the bulk aerodynamic relationship.

The behavior of the subgrid velocity scale is estimated from five different field programs. The first part of the subgrid velocity scale is formulated in terms of subgrid variability of the surface radiative temperature [(24) and (25)] to represent generation of subgrid motions by surface heterogeneity. This term is dominant in the CODE flight 19 data. The second part of the subgrid velocity scale, due primarily to background transient mesoscale motions, is formulated as a function of grid size [Eq. (26)]. Larger grid size corresponds to a larger range of unresolved subgrid motions.

This study also briefly examines the bulk aerodynamic relationship based on a generalized velocity scale expressed in terms of the free convection velocity scale as in Godfrey and Beljaars (1991), Stull (1994), and Beljaars (1995). Here, the free convection velocity scale accounts for flux associated with buoyancy-driven boundary-layer-scale motions. As is shown in section 2, this approach is analytically (but not quantitatively) equivalent to modifying the stability function of the exchange coefficient and can be derived by time averaging the instantaneous wind speed. This generalization of the bulk aerodynamic relationship reduces the scale dependence of the exchange coefficient for the case of weak winds and significant surface heating.

Since the subgrid and free convection velocity scales significantly reduce the dependence of the exchange coefficient on averaging scale (grid size), local similarity theory might be used to estimate the effective exchange coefficient in the generalized bulk aerodynamic formulation [Eq. (27)]. The generalization of the velocity scale will have little impact on the prediction of fluxes in the case of significant large-scale flow but becomes important when the large-scale flow is weaker than a few meters per second. As a simpler alternative, this study lends some support to simply specifying a minimum wind speed in large-scale models. At a slightly higher level of sophistication, the minimum wind speed could be specified to increase with grid size using (26).

The above analysis requires more data for cases of weak large-scale flow, organized mesoscale circulations (sea breezes, moist convective systems), and the nocturnal boundary layer where subgrid slope circulations are sometimes stronger than the large-scale flow. The formulations developed here are conservative estimates of the subgrid velocity scale since the data include mainly background mesoscale motions without strong organized convective systems. However, the effect of such stronger systems on subgrid-scale transport may not yield to simple formulation.

REFERENCES

Avissar, R., 1990: Operating ranges of mesoscale numerical models and meteorological wind tunnels for the simulation of sea and land breezes. *Bound.-Layer Meteor.,* **50,** 227–275.

——, and R. A. Pielke, 1989: A parameterization of heterogeneous land surfaces for atmospheric numerical models and its impact on regional meteorology. *Mon. Wea. Rev.,* **117,** 2113–2136.

Beljaars, A. C., 1995: The parameterization of surface fluxes in large scale models under free convection. *Quart. J. Roy. Meteor. Soc.,* **121,** 255–270.

Businger, J. A., 1973: A note on free convection. *Bound.-Layer Meteor.,* **4,** 322–326.

Claussen, M., 1991: Estimation of areally-averaged surface fluxes. *Bound.-Layer Meteor.,* **54,** 387–410.

Ducoudré, N. I., K. Laval, and A. Perrier, 1993: SECHIBA, a new set of parameterizations of the hydrologic exchanges at the land–atmosphere interface within the LMD atmospheric general circulation model. *J. Climate,* **6,** 248–273.

Esbensen, S. K., and R. W. Reynolds, 1981: Estimating monthly averaged air–sea transfers of heat and momentum using the bulk aerodynamic method. *J. Phys. Oceanogr.,* **11,** 457–465.

Godfrey, J. S., and A. C. M. Beljaars, 1991: On the turbulent fluxes of buoyancy, heat and moisture at the air–sea interface at low wind speeds. *J. Geophys. Res.,* **96,** 22 043–22 048.

Hadfield, M. G., W. R. Cotton, and R. A. Pielke, 1992: Large-eddy simulations of thermally forced circulations in the convective

boundary layer. Part II: The effect of changes in wavelength and wind speed. *Bound.-Layer Meteor.,* **58,** 307–327.

Hechtel, L. M., C.-H. Moeng, and R. B. Stull, 1990: The effects of nonhomogeneous surface fluxes on the convective boundary layer: A case study using large-eddy simulation. *J. Atmos. Sci.,* **47,** 1721–1741.

Huang, X., and T. J. Lyons, 1995: The simulation of surface heat fluxes in a land surface–atmosphere model. *J. Appl. Meteor.,* **34,** 1099–1111.

Liu, W. T., K. B. Katsaros, J. A. Businger, and J. E. Tillman, 1979: Heat transport and thermal structure in the interfacial boundary layer measured in an open tack of water in turbulent free convection. *J. Atmos. Sci.,* **36,** 1722–1735.

Louis, J.-F., 1979: A parametric model of vertical eddy fluxes in the atmosphere. *Bound.-Layer Meteor.,* **17,** 187–202.

Lyons, T. J., P. Schwerdtfeger, J. M. Hacker, I. J. Foster, R. C. G. Smith, and X. Huang, 1993: Land–atmosphere interaction in a semi-arid region: The bunny fence experiment. *Bull. Amer. Meteor. Soc.,* **74,** 1327–1324.

MacPherson, J. I., 1992: NRC Twin Otter operations in the 1991 California Ozone Deposition Experiment. Rep. LTR-FR-118. Flight Research Laboratory, National Research Council, Ottawa, Canada.

Mahrt, L., 1991: Eddy asymmetry in the sheared heated boundary layer. *J. Atmos. Sci.,* **48,** 472–492.

——, and J. Sun, 1995: Dependence of exchange coefficients on averaging scale or grid size. *Quart. J. Roy. Meteor. Soc.,* submitted.

——, I. MacPherson, and R. Desjardins, 1994a: Observations of fluxes over heterogeneous surfaces. *Bound.-Layer Meteor.,* **67,** 345–367.

——, J. Sun, D. Vickers, J. I. MacPherson, J. R. Pederson, and R. L. Desjardins, 1994b: Observations of fluxes and inland breezes over a heterogeneous surface. *J. Atmos. Sci.,* **51,** 2165–2178.

Miller, M. J., A. C. M. Beljaars, and T. N. Palmer, 1992: The sensitivity of the ECMWF model to the parameterization of evaporation from the tropical oceans. *J. Climate,* **5,** 418–434.

NASA, 1994: *Experiment Plan; Boreal Ecosystem–Atmospheric Study.* NASA Goddard Space Flight Center, 577 pp.

Segal, M., and R. W. Arritt, 1992: Non-classical mesoscale circulations caused by surface sensible heat flux gradients. *Bull. Amer. Meteor. Soc.,* **73,** 1593–1604.

Schumann, U., 1988: Minimum friction velocity and heat transfer in the rough surface layer of a convective boundary layer. *Bound.-Layer Meteor.,* **44,** 311–326.

Stull, R. B., 1994: A convective transport theory for surface fluxes. *J. Atmos. Sci.,* **51,** 3–22.

Sugita, M., and W. Brutsaert, 1990: Regional surface fluxes from remotely sensed skin temperature and lower boundary layer measurements. *Water Resour. Res.,* **26,** 2937–2944.

Sun, J., and L. Mahrt, 1994: Spatial distribution of surface fluxes estimated from remotely sensed variables. *J. Appl. Meteor.,* **33,** 1341–1353.

——, and ——, 1995: Determination of surface fluxes from the surface radiative temperature. *J. Atmos. Sci.,* **52,** 1096–1106.

Sykes, R. I., D. S. Henn, and W. S. Lewellen, 1993: Surface-layer description under free-convection conditions. *Quart. J. Roy. Meteor. Soc.,* **119,** 409–421.

TOGA COARE International Project Office, 1993: TOGA COARE Intensive Observing Period Operations Summary, June, 1993. TOGA COARE International Project Office, UCAR, Boulder, CO, 610 pp.

Tucker, C. J., 1979: Red and photographic infrared linear combinations for monitoring vegetation. *Remote Sens. Environ.,* **8,** 127–150.

Wetzel, P. J., and J.-T. Chang, 1988: Evapotranspiration from non-uniform surfaces: A first approach for short-term numerical weather prediction. *Mon. Wea. Rev.,* **116,** 600–621.